Study of Perfusion Kinetics in Human Brain Tumor Using Leaky Tracer Kinetic Model of DCE-MRI Data and CFD

A. Bhandari[1], A. Bansal[2], A. Singh[3,4], and N. Sinha[1(✉)]

[1] Department of Mechanical Engineering,
Indian Institute of Technology, Kanpur 208016, India
nsinha@iitk.ac.in
[2] Department of Mechanical and Industrial Engineering,
Indian Institute of Technology, Roorkee 247677, India
[3] Centre for Biomedical Engineering, Indian Institute of Technology,
New Delhi 110016, India
[4] Department of Biomedical Engineering,
All India Institute of Medical Sciences, New Delhi 110016, India

Abstract. A computational fluid dynamics (CFD) model based on realistic voxelized representation of human brain tumor vasculature is presented. The model utilizes dynamic contrast enhanced magnetic resonance imaging (DCE-MRI) data to account for heterogeneous porosity and permeability of contrast agent inside the tumor. Patient specific arterial input function (AIF) is employed in this study. Owing to higher accuracy of Leaky Tracer Kinetic Model (LTKM) in shorter duration human imaging data, the model is employed to determine perfusion parameters and compared with General Tracer Kinetic Model (GTKM). The developed CFD model is used to simulate and predict transport, distribution and retention of contrast agent in different parts of human tissue at different times. In future, a patient specific model can be developed to forecast the deposition of drugs and nanoparticles and tune the parameters for thermal ablation of tumors.

Keywords: Voxelized model · Human brain tumor · AIF · LTKM · GTKM · DCE-MRI · CFD

1 Introduction

Cancer, a deadly disease occurs as a consequence of abnormal cell growth. It is the leading cause of human's death in developed as well as developing countries [1]. Most of the human cancers are solid tumors (approximately 85%) [2]. These tumors depend on other normal tissues for their nutritional material and thus grow in size. Chemotherapy and hyperthermia are widely used for cancer treatment. However, physicochemical properties of drug and biological properties of tumors put many limitations in all treatment strategies. Limited penetration of drug to tumor cells and difficulty in targeting sufficient amount of heat only to tumor tissue are the primary reasons of failure of chemotherapy and hyperthermic treatment respectively. On the other hand,

M. Fei et al. (Eds.): LSMS/ICSEE 2017, Part I, CCIS 761, pp. 63–73, 2017.
DOI: 10.1007/978-981-10-6370-1_7

biological properties of tumors such as irregular vasculature, impaired lymphatic system and hypoxic conditions also lead to failure of these treatments [3]. Therefore, there is an urgent need to have proper knowledge of transport barriers that the drug or a drug carrying nanoparticle encounters when administered systematically inside a human's body. To this end, mathematical models are an excellent tool in investigating these transport barriers.

In order to study the transport barriers, Baxter and Jain developed a theoretical model to analyze a uniform as well as non-uniform perfused tumor. They demonstrated the effect of interstitial fluid pressure (IFP) and necrotic core on drug delivery [4, 5]. Soltani and Chen developed a homogenous tumor model and concluded that IFP becomes less than the effective pressure below the critical tumor radius, which makes the chemotherapeutic drug transport to tumor site easier [6]. Wang *et al.* used two different drug delivery modes to simulate the delivery of carmustine to brain tumors and concluded that polymeric drug delivery is better [7]. Pishko *et al.* modelled the drug delivery through the tumor tissue by using magnetic resonance imaging (MRI) technique and demonstrated the effects of heterogeneous vasculature and porosity [8]. Later, Magdoom *et al.* came out with a voxelized approach to model the drug delivery process that helped in reducing the computational time and increased accuracy [9]. Zhan *et al.* modeled the delivery of thermo-sensitive liposomes to solid tumors and concluded that thermo-sensitive liposome delivery leads to higher intracellular concentration of drug, enhancing the therapeutic effect of the drug [10].

All the above mentioned models have unfolded new insights in understanding the transport process that can be extended to study the transport of nanoparticles for thermal ablation of tumors. However, the assumption of spherical shape and homogeneous vasculature are far from reality. Studies incorporating heterogeneous vasculature of tumors too had mostly focused on animal models with Simple Tofts Model and global arterial input function (AIF), which is time dependent concentration of tracer in blood plasma.

The main objective of the present study is to model the interstitial fluid flow parameters (pressure and velocity) and tracer transport in realistic human brain tumors with help of DCE-MRI data. Heterogeneous vasculature of tumor and spatially varying permeability and porosity have been taken into account. In addition, local or patient specific AIF has been measured and used for accurate determination of the perfusion parameters. General Tracer Kinetic Model (GTKM) [11] also called Extended Tofts Model has been employed for calculation of permeability and porosity maps. This model has been used because blood volume fraction in case of human tumors is quite large and this is taken care of by including intravascular term in this model [12]. In addition to the GTKM model, Leaky Tracer Kinetic Model (LTKM) [13] has also been used for generating perfusion parameters. CFD results (IFP, Interstitial fluid velocity (IFV) and tracer concentration) have been obtained by using perfusion parameters from both the models and are compared with experimental DCE-MR results. To the best of authors' knowledge, this is the first study related to CFD analysis of realistic human brain tumors based on DCE-MRI data and LTKM.

2 Data and Methodology

To obtain the permeability and porosity maps of tumor, a compartment model is fitted to the DCE-MRI data. The GTKM model assumes that tissue is divided into two compartments: plasma space and extravascular extracellular space (EES), also called interstitial space. It assumes bidirectional exchange of contrast agent from plasma space to EES. Contrast agent from plasma compartment permeates into EES. This model basically calculates the three important perfusion parameters namely rate transfer constant from plasma space to EES (K^{trans}), fractional plasma volume (v_p) and fractional EES volume or porosity (v_e). On the other hand, LTKM is a three compartment model in which three compartments are plasma, permeable and leakage compartments. This model basically assumes that EES is composed of two compartments permeable space and leakage space. In permeable space bidirectional exchange of contrast agent takes place where as in leakage space only unidirectional exchange of contrast agent occurs i.e. contrast does not flow back to vasculature. Figure 1 gives a clear picture of these two models depicting only bidirectional exchange in GTKM and unidirectional as well as bidirectional exchange in LTKM.

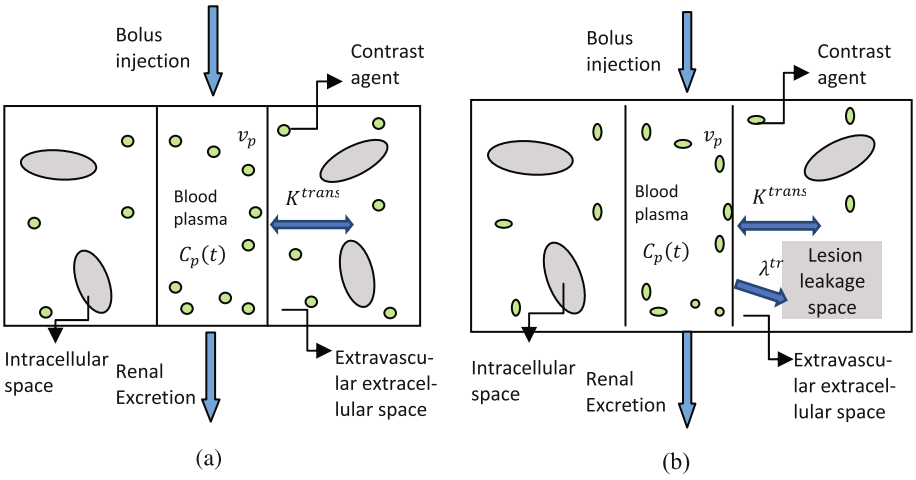

Fig. 1. Schematic of both models (a) GTKM (b) LTKM

2.1 MR Imaging and 3D Porous Media Computational Model

DCE-MR imaging was performed on a 3.0T Ingenia MRI scanner (Philips Healthcare, The Netherlands). Written consent from each patient was obtained before MRI study. Imaging was performed using a fast field echo (T1-FFE) sequence (TR/TE = 4.38 ms/2.3 ms, flip angle = 10°, field of view (FOV) = 240 × 240 mm^2, slice thickness = 6 mm, matrix size = 256 × 256). A dose of 0.1 mmol/kg body weight of Gd-BOPTA (Gadobenate Dimeglumine) (Multihance, Bracco, Italy) was administered intravenously with the help of a power injector. A total of 384 images at 32 time points

for 12 slices were acquired with a temporal resolution approximately of 4 s for each time point. From DCE-MRI images, contrast concentration on each voxel was calculated from signal intensity with the help of SPGR/FFE signal equation. Pre contrast T1 (T10) was estimated using 3 fast spin echo (FSE) image (T1 - weighted, T2 - weighted, and proton density - weighted) [14]. The longitudinal and transverse relaxivity ($R_1$and R_2) of contrast agent in body were taken as 6.3 $mmol^{-1}s^{-1}L$ and 17.5 $mmol^{-1}s^{-1}L$ respectively [15]. Local AIF was estimated using a method described by Singh et al. [16]. These concentration values obtained from Eq. (1) are used to fit Eqs. (2) and (3) i.e. two compartment model and three compartment model respectively. Equations (1, 2 and 3) are listed in Table 1. The second and third equations listed in Table 1 are fitted to get perfusion parameter maps (K^{trans}, v_e, v_p) by GTKM and ($K^{trans}, v_e, v_p, \lambda^{tr}$) by LTKM at each voxel respectively. The perfusion parameter maps got from both the models were imported in 3D porous media model made in OpenFOAM. Porous media model used in this study consists of fluid flow and tracer transport equations and has been described in our previous study [17].

Table 1. Equations used for analysis of MR images

Name of Equation	Equation
1. SPGR/FFE Signal Equation	$\frac{S(t)}{S(0)} = k_0 \exp(-TER_2 C(t)) \frac{1-\exp\left(-TR(T_{10}^{-1}+R_1 C(t))\right)}{1-\cos(\theta)\exp\left(-TR(T_{10}^{-1}+R_1 C(t))\right)}$ Where $k_0 = \frac{1-\cos(\theta)\exp\left(-TRT_{10}^{-1}\right)}{1-\exp\left(-TRT_{10}^{-1}\right)}$
2. General tracer kinetic model	$C_t = v_p C_p(t) + K^{trans} \int_0^t C_p(\tau) e^{\frac{K^{trans}}{v_e}(\tau - t)} d\tau$
3. Leaky tracer kinetic model	$C_t = v_p C_p(t) + K^{trans} \int_0^t C_p(\tau) e^{\frac{K^{trans}}{v_e}(\tau - t)} d\tau + \lambda^{tr} \int_0^t C_p(\tau) d\tau$

Where, S (0) is the signal intensity when no contrast agent is given, S (t) is the signal intensity at a particular time point, **TE** is the echo time (msec), **TR** is the repetition time (msec), **θ** is the flip angle, $\boldsymbol{C_t}$ is the total tissue contrast agent concentration (mmol/Lt), $\boldsymbol{C_p(t)}$ is the time dependent concentration of contrast agent in blood plasma (mmol/Lt) and $\boldsymbol{\lambda^{tr}}$ is the rate transfer constant between plasma and leakage compartment.

For reduction in the computational time, only the tumor part and the surrounding brain normal tissue were modelled. A rectangular volume of size 40 × 36 × 72 mm^3 enclosing the tumor and the normal tissue was created and meshed using the OpenFOAM software. The mesh element size in the rectangular volume was same as that of voxel size in MRI slice (0.9375 × 0.9375 × 6 mm^3). The values of tracer kinetic parameters obtained from both the models were entered at each voxel inside the OpenFOAM CFD model. The SIMPLE (semi implicit method for pressure linked equations) algorithm [18] was used and standard interpolation schemes used by OpenFOAM were used to discretize the equations. Zero fluid pressure boundary conditions were applied at all the boundaries. Zero gradient boundary conditions were applied for interstitial fluid velocity and concentration of contrast agent. Initial

condition for contrast agent transport was set to zero ($C_t = 0$). Grid independence test was done to see the effect of change in mesh size on the simulated tracer concentration. Increasing the number of mesh elements to four times the original value resulted in less than 3% change in tracer concentration.

3 Results and Discussion

Pre-contrast and post-contrast images of brain of one slice are shown in Fig. 2(a), (b) respectively. Local or patient specific AIF used in this study is shown in (Fig. 2(c)).

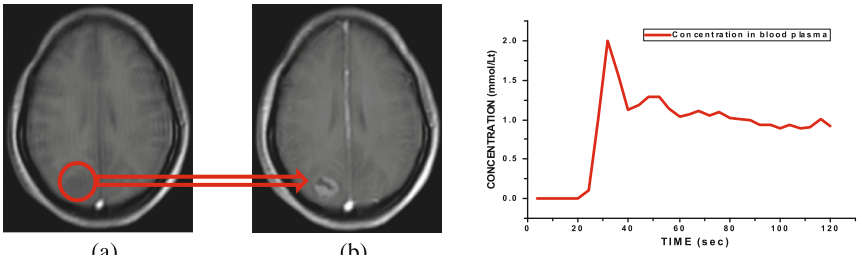

Fig. 2. MR images of brain (a) Pre contrast (b) Post contrast (c) AIF of the patient

Permeability and porosity maps of a particular slice (slice 10) obtained by fitting DCE-MRI data to both the models (GTKM and LTKM) are shown in Fig. 3. As can be observed, perfusion parameters obtained from both the models have significant difference. K^{trans} and porosity maps derived from LTKM were found to be more heterogeneous as compared to those got from GTKM. Figure 4 shows the contour plots of IFP and IFV, showing no significant difference in the values obtained from both the models. Figure 4(a) shows higher IFP inside the tumor with value equal to 1530 Pa, which rapidly decreased at the tumor boundary. IFV contour plot (Fig. 4(b)) was completely reverse of IFP with higher values of 0.04 μm/s at the tumor periphery. Simulated values of IFP and IFV were validated with the experimental values previously measured in the literature for human brain tumors [19, 20]. The higher and uniform value of IFP within the tumor is responsible for negligible convective transport of tracer within the tumor interstitium. Transport of tracer within tumor interstitium takes place mainly by diffusion. Convective transport of tracer is only significant at the periphery of tumor. This is due to the reason of steep pressure gradient and higher IFV at the tumor periphery, which helps in outward convection of tracer from the tumor.

Next, the interstitial tracer concentration was simulated using perfusion parameters of both the models. The tracer concentration simulation was carried out for two minutes since experimental data was available only for two minutes.

The comparison with experimental data was done at 14^{th} time point (56 s) and 28^{th} time point (112 s). Figure 5 shows contour plots of the tracer concentration simulated by using perfusion parameters of both the models (GTKM and LTKM) and

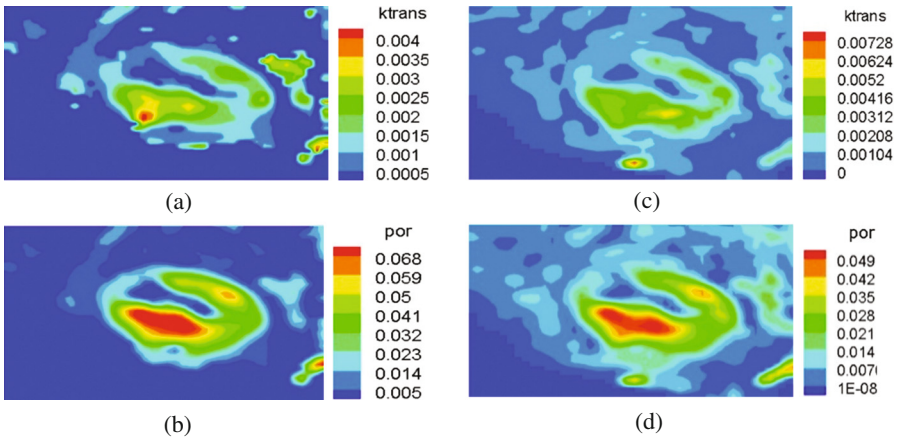

Fig. 3. Contour plots of perfusion parameters by GTKM (a) Permeability (K^{trans} (sec^{-1})) maps (b) Porosity (v_e) maps and LTKM (c) Permeability (K^{trans} (sec^{-1})) maps (d) Porosity (v_e) maps.

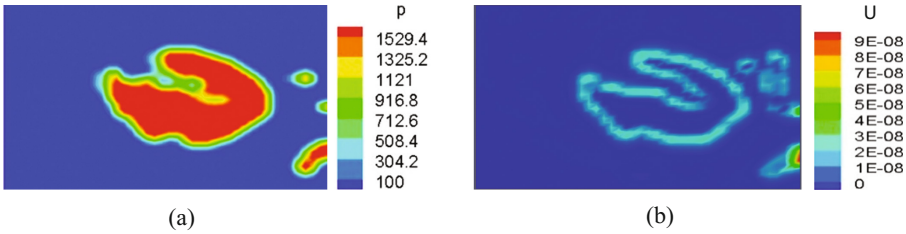

Fig. 4. Contour plots of (a) Interstitial fluid pressure (IFP) and (b) Interstitial fluid velocity (IFV).

experimental data at both the time points. As seen from contour plots tracer concentration obtained from LTKM perfusion parameters was more heterogeneous and more close to experimental results qualitatively. To make quantitative comparison, line plots were plotted along the horizontal and vertical bisector of the slice for both time points. Line plots of tracer concentration give an accurate picture of how closely the simulated results overlap with experimental ones. Figure 6 shows line plots of tracer concentration (both experimental and simulated) at horizontal and vertical bisector for 14^{th} and 28^{th} time points.

It is clear from line plots that simulated tracer concentration from LTKM obtained perfusion parameters was much close and correlates well with experimental concentration as compared to GTKM obtained perfusion parameters. Similar analysis was done on three more tumor data sets. Similar results were obtained, with simulated concentration from LTKM obtained perfusion parameters being more close to experiments. Tracer concentration peaks at tumor site in approximately 90–100 s after the administration intravenously, and then contrast begins to wash out from tumor site.

However, the wash out rate found in this tumor can't be extrapolated to other tumors as it highly depends on the type and characteristics such as size, grade and volume of tumors. It can be concluded that the developed computational model accurately captures the tracer concentration in tissues qualitatively as well as quantitatively. Further, the LTKM model gives more accurate perfusion parameters for short duration MRI data, as used in this study, which further help in predicting more accurate tracer concentration by CFD. For short duration MRI data, the GTKM model does not give correct estimation of volume fraction of extravascular extracellular space (EES) or porosity [13]. For correct estimation of porosity, data acquisition is suggested to be long enough for concentration of contrast agent to become stabilized (approximately 15–20 min) [21]. This is not always possible in case of clinical data due to many issues such as long scan time and blurring of image caused due to motion of patient over long time leading to inaccurate analysis. Also porosity and K^{trans} values in the GTKM model keep on varying with time for contrast enhancing tissues, which is not the case with LTKM. By changing temporal resolution of DCE-MR scans GTKM gives varying estimates of perfusion parameters whereas with LTKM, the perfusion parameters remain constant [13]. Thus, for shorter duration of MRI data, LTKM is preferable and provides better estimate of perfusion parameters. To further confirm the accuracy of results, a statistical analysis was performed. Root mean square (RMS) error and Pearson product moment correlation coefficient (PPMCC) were calculated along the values at horizontal and vertical bisector for both the time points as shown in Table 2.

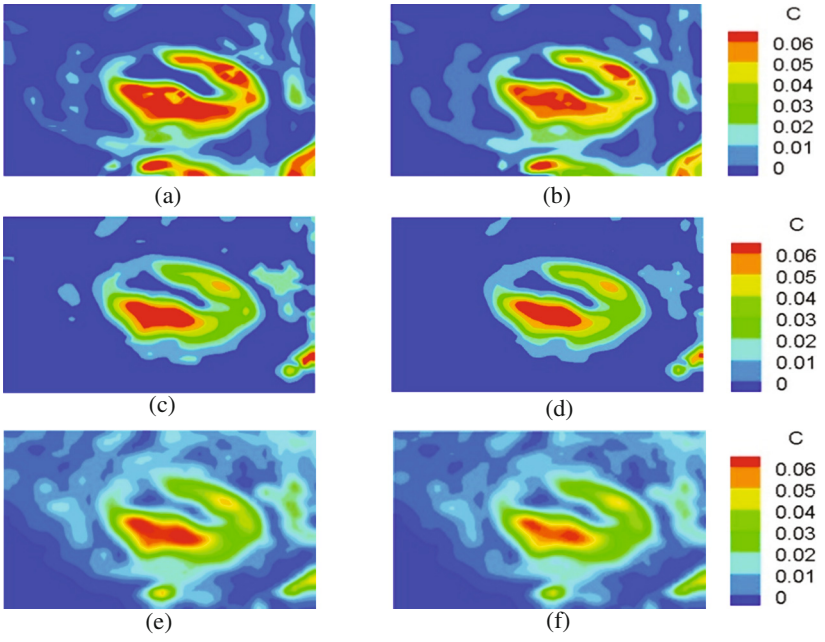

Fig. 5. Contour plots of tracer concentration at 14th time point (56 s) (a) Experimental (c) Simulated with GTKM perfusion parameters (e) Simulated with LTKM perfusion parameters and at 28th time point (112 s) (b) Experimental (d) Simulated with GTKM perfusion parameters (f) Simulated with LTKM perfusion parameters. Units of concentration are mmol/Lt.

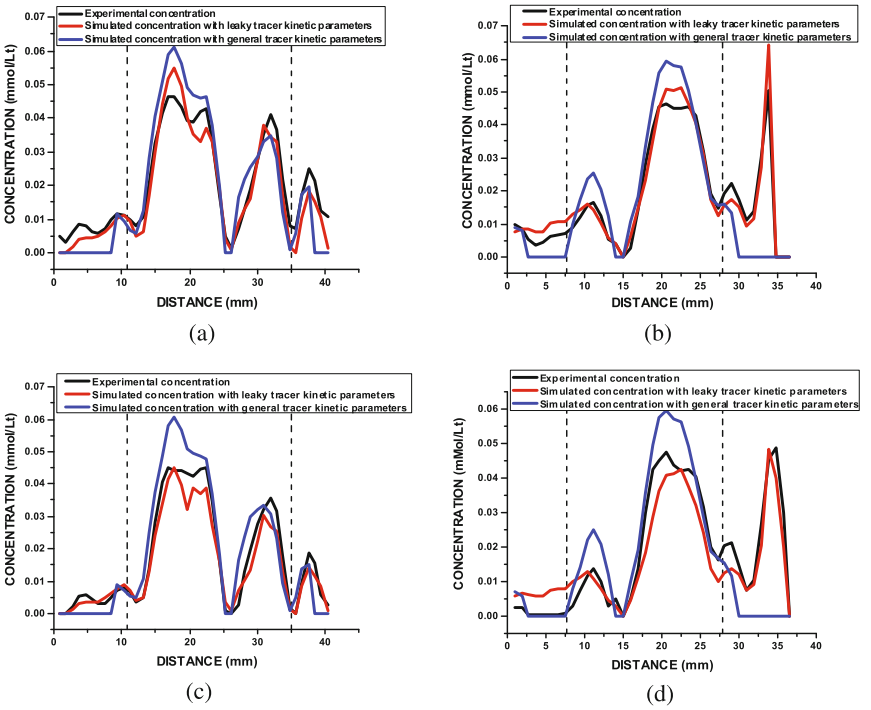

Fig. 6. Line plots of tracer concentration at 14th time point (56 s) (a) Horizontal Bisector (b) Vertical Bisector and at 28th time point (112 s) (c) Horizontal Bisector (d) Vertical Bisector

Table 2. Statistical analysis comparing Experimental and Simulated results

Variable	Model	Quantity	RMS error	PPMCC
C_t	Tracer concentration simulated with GTKM perfusion parameters	t = 14th time point		
		Horizontal Bisector	0.0079 mmol/Lt	0.91055
		Vertical Bisector	0.0155 mmol/Lt	0.74357
		t = 28th time point		
		Horizontal Bisector	0.0071 mmol/Lt	0.91944
		Vertical Bisector	0.0143 mmol/Lt	0.70202

(*continued*)

Table 2. (*continued*)

Variable	Model	Quantity	RMS error	PPMCC
	Tracer concentration simulated with LTKM perfusion parameters	$t = 14^{th}$ time point		
		Horizontal Bisector	0.0044 mmol/Lt	0.97273
		Vertical Bisector	0.0036 mmol/Lt	0.97731
		$t = 28^{th}$ time point		
		Horizontal Bisector	0.0041 mmol/Lt	0.98563
		Vertical Bisector	0.0060 mmol/Lt	0.95278

RMS error decreased by 44% and 76% at 14^{th} time point and by 38% and 58% at 28^{th} time point along horizontal and vertical bisector respectively when tracer concentration was simulated using LTKM parameters. Tracer concentration simulated with help of LTKM parameters always show a good correlation (>0.9) at both time points and for both bisectors as compared to those simulated with GTKM parameters.

4 Conclusions

A computational model based on DCE-MRI data was developed to study transport of contrast agent in realistic heterogeneous human brain tumor. Two different models (GTKM and LTKM) were used to obtain perfusion parameters. Simulated contrast agent concentration obtained by LTKM perfusion parameters showed better agreement with the experimental MRI data as compared to those obtained by GTKM perfusion parameters. Also, simulated IFP and IFV values correlated well with experimentally measured human brain tumor values reported in literature. The developed model is patient specific and can be used to select the most suitable chemotherapeutic drug for a specific patient before starting the treatment. Moreover, the developed CFD model in future can be used to predict the deposition of nano-particle encapsulated drugs. Once the deposition of nano particles in tumor area is known the porous media transport model used in this study can be coupled with heat transfer equations to study the effect of hyperthermic treatment in tumor microenvironment [22].

Acknowledgements. The authors would like to thank Dr. R.K. Gupta for providing clinical data, Prof. R.K.S. Rathore and Dr. Prativa Sahoo for technical support in DCE-MRI data analysis. This research was supported by grants from IIT Kanpur and Science and Engineering Research Board (grant number: YSS/2014/000092).

References

1. Siegel, R., Naishadham, D., Jernal, A.: Cancer statistics, CA cancer. J. Clin. **63**, 11–30 (2013)
2. Jain, R.K.: Normalization of tumor vasculature: an emerging concept in antiangiogenic therapy. Science **307**, 58–62 (2005)
3. Etryk, A.A., Giustini, A.J., Gottesman, R.E., Kaufman, P.A., Jack Hoopes, P.: Magnetic nanoparticle hyperthermia enhancement of cisplatin chemotherapy cancer treatment. Int. J. Hypertherm. **29**, 845–851 (2013)
4. Baxter, L.T., Jain, R.K.: Transport of fluid and macromolecules in tumors. I. Role of interstitial pressure and convection. Microvasc. Res. **37**(1), 77–104 (1989)
5. Baxter, L.T., Jain, R.K.: Transport of fluid and macromolecules in tumors. II. Role of heterogeneous perfusion and lymphatics. Microvasc. Res. **40**(1), 246–263 (1990)
6. Soltani, M., Chen, P.: Numerical modeling of fluid flow in solid tumors. PLoS ONE **6**(6), e20344 (2011)
7. Wang, C.H., Li, J., Teo, C.S., Lee, T.: The delivery of BCNU to brain tumors. J. Control Release **61**, 21–41 (1999)
8. Pishko, G.L., Astary, G.W., Mareci, T.H., Sarntinoranont, M.: Sensitivity analysis of an image based solid tumor computational model with heterogeneous vasculature and porosity. Ann. Biomed. Eng. **39**(9), 2360–2373 (2011)
9. Magdoom, K.N., Pishko, G.L., Kim, J.H., Sarntinoranont, M.: Evaluation of a voxelized model based on DCE-MRI for tracer transport in tumor. J. Biomech. Eng. **134**, 091004 (2012)
10. Zhan, W., Xu, X.Y.: A mathematical model for thermo-sensitive liposomal delivery of doxorubicin to solid tumour. J. Drug Del., Article ID 172529 (2013)
11. Tofts, P.S., Parker, G.J.M., DCE-MRI: acquisition and analysis techniques. In: Clinical Perfusion MRI: Techniques and Applications, pp. 58–74 (2013)
12. Parker, G.J.M., Buckley, D.L.: Tracer kinetic modelling for T1-weighted DCE-MRI. In: Jackson, A., Buckley, D.L., Parker, G.J.M. (eds.) Dynamic Contrast-Enhanced Magnetic Resonance Imaging in Oncology. Medical Radiology (Diagnostic Imaging), pp. 81–92. Springer, Heidelberg (2005). 10.1007/3-540-26420-5_6
13. Sahoo, P., Rathore, R.K.S., Awasthi, R., Roy, B., Verma, S., Rathore, D., Behari, S., Husain, M., Husain, N., Pandey, C.M., Mohakud, S., Gupta, R.K.: Sub compartmentalization of extracellular extravascular space (EES) into permeability and leaky space with local arterial input function (AIF) results in improved discrimination between high- and low-grade glioma using dynamic contrast-enhanced (DCE) MRI. J. Magn. Reson. Imaging **38**, 677–688 (2013)
14. Singh, A., Haris, M., Purwar, A., Sharma, M., Husain, N., Rathore, R.K.S., Gupta, R.K.: Quantification of physiological and hemodynamic indices using T1 DCE-MRI in intracranial mass lesions. J. Magn. Reson. Imaging **26**, 871–880 (2007)
15. Pintaske, J., Martirosian, P., Graf, H., Erb, G., Lodemann, K.P., Claussen, C.D., Schick, F.: Relaxivity of gadopentetate dimeglumine (magnevist), gadobutrol (gadovist), and gadobenate dimeglumine (multihance) in human blood plasma at 0.2, 1.5 and 3 tesla. Investigat. Radiol. **41**(3), 213–221 (2006)
16. Singh, A., Rathore, R.K.S., Haris, M., Verma, S.K., Husain, N., Gupta, R.K.: Improved bolus arrival time and arterial input function estimation for tracer kinetic analysis in DCE-MRI. J. Magn. Reson. Imaging **29**, 166–176 (2009)
17. Bhandari, A., Bansal, A., Singh, A., Sinha, N.: Perfusion kinetics in human brain tumor with DCE-MRI derived model and CFD analysis. J. Biomech. **59**, 80–89 (2017)

18. Anderson, D.A., Tannehill, J.C., Pletcher, R.H.: Computational Fluid Mechanics and Heat Transfer, pp. 671–674. Hemisphere, New York (1984)
19. Jain, R.K.: Delivery of molecular and cellular medicine to solid tumors. Adv. Drug Deliv. Rev. **46**, 149–168 (2001)
20. Guttman, R., Leunig, M., Feyh, J., Goetz, A.E., Messmer, K., Kastenbauer, E.: Interstital hypertension in head and neck tumors in patients: correlation with tumor size. Cancer Res. **52**, 1993–1995 (1992)
21. Donaldson, S.B., West, C.M., Davidson, S.E., Carrington, B.M., Hutchison, G., Jones, A.P., Sourbron, S.P., Buckley, D.L.: A comparison of tracer kinetic models for T1 weighted dynamic contrast enhanced MRI: applications in carcinoma of the cervix. Magn. Reson. Med. **63**, 691–700 (2010)
22. Nabil, M., Decuzzi, P., Zunino, P.: Modeling mass and heat transfer in nano-based cancer hyperthermia. R. Soc. Open Sci. **2**, 150447 (2015)